Inferring spatial variations in velocity profiles and bed geometry of natural debris flows based on discharge estimates from high-frequency 3D LiDAR point clouds; Illgraben, Switzerland

Raffaele Spielmann[1,2*], *Jordan* Aaron[1,2], and *Brian W.* McArdell[2]

[1]ETH Zürich, Department of Earth Sciences, Engineering Geology, 8092 Zurich, Switzerland
[2]Swiss Federal Institute for Forest, Snow and Landscape Research WSL, 8903 Birmensdorf, Switzerland

Abstract. More detailed field measurements are required for a better understanding of surging debris flows. In this work, we analyze a debris flow at the field-scale using timelapse point clouds from a high-resolution, high-frequency 3D LiDAR sensor, which has been installed over a check dam on the fan of the Illgraben catchment in Switzerland. In our investigations, we manually measured the front velocity and tracked individual features such as large boulders and woody debris over a 25 m long channel segment. We observed a change in the front velocity as well as a difference in the velocity of large boulders and woody debris ($v_{boulder} \approx 0.6 \ v_{wood}$) during the second surge of the event. We also estimated the discharge for different closely spaced channel sections based on automated measurements of the cross-sectional area and the surface velocity, which enabled us to infer spatial variations in the bed geometry and the velocity profile. From the discharge estimates, we then derived the volume of this event. Over the course of the next year, the amount of field-scale LiDAR data from the Illgraben will increase substantially and allow for an even more detailed analysis of fundamental debris-flow processes.

1 Introduction

The destructiveness of debris flows is strongly controlled by their surging behavior, which manifests as peak discharge values being order of magnitudes larger than floods [1, 2]. This surging behavior is not fully understood at present and more detailed field measurements are needed to clarify this process [3, 4]. In particular, high temporal and spatial resolution measurements of front and surface velocity as well as event discharge are needed to better understand debris-flow destructiveness. In the present work, we quantify the following of these hazard-related parameters in unprecedented detail at the field scale using a newly installed 3D timelapse LiDAR scanner: (*i*) front velocity, (*ii*) surface velocity, (*iii*) cross-sectional area, (*iv*) discharge and (*v*) event volume.

In the past, debris-flow front velocity has been quantified using time-distance methods, video sequence analysis or high-frequency radar measurements [5]. Other researchers have studied the velocity profile present in debris-flow material and have shown that it can vary from block sliding to simple shear [6, 7]. Furthermore, debris-flow discharge has been investigated at many locations worldwide [5]. These studies have revealed that discharge can vary strongly through time due to the surging nature of these flows.

In the present study, we use a high-resolution, high frequency (10 Hz), multi-beam LiDAR scanner (*Ouster* OS1-64, Gen. 1; see also [8]), which has the distinct

advantage – especially over the abovementioned, conventional monitoring techniques – of capturing an undistorted, truly 3D representation of the surroundings, even in the absence of light or during rainfall. Such a LiDAR scanner has been installed in Switzerland's Canton of Valais at the Illgraben, one of the most active debris-flow catchments in the Alps [9]. The monitoring station is located roughly 500 m downstream of the fan apex, and the sensor is suspended in the middle of the channel above a check dam (Fig. 1). On 19 September 2021, the LiDAR scanner recorded a first debris-flow event, which will be analyzed herein.
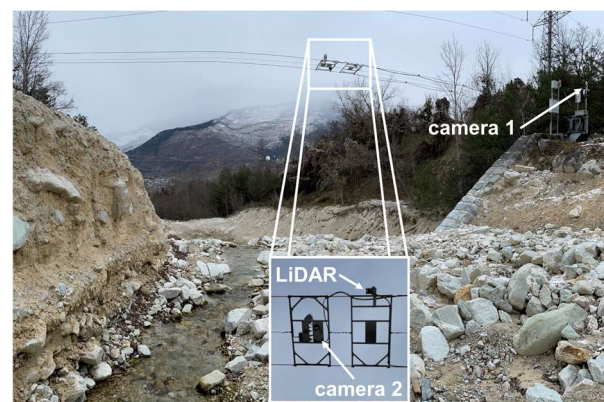

Fig. 1. LiDAR scanner (*Ouster* OS1-64, Gen. 1) and video cameras at the monitoring station "Gazoduc", which is located on the fan of the Illgraben next to a check dam, ca. 500 m downstream of the apex.

---

* Corresponding author: raffaele.spielmann@erdw.ethz.ch

2 Methods

The first step was pre-processing the raw point clouds, i.e. all point-cloud frames of the 19 Sept. 2021 event. In this step, the point clouds were rotated around the mean slope of the channel segment upstream of the sensor (3.70°) to a bed-parallel coordinate system. Afterwards, the point clouds were cropped to a 50 m x 20 m x 8 m box to omit reflections from objects outside of the channel bed (e.g. trees).

Because the shape of the channel bed during the debris-flow event is unknown (erosion or deposition), we prepared different *channel geometry scenarios* to account for this uncertainty when measuring the cross-sectional area (cf. also [10]). For each section, a *pre-event* and *post-event* channel geometry was defined based on LiDAR scans recorded immediately before and after the event, respectively. Furthermore, we specified a third, *intermediate* channel geometry which served as "mean" scenario for these measurements (Fig. 2a).
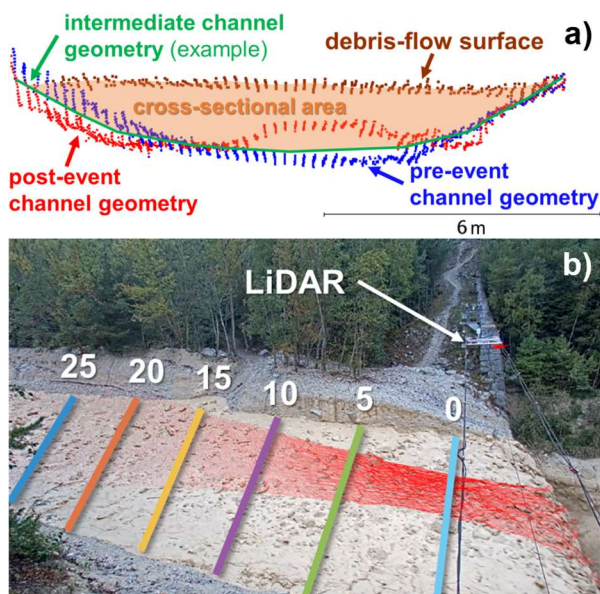

Fig. 2. a) Channel section ca. 25 m upstream of the LiDAR sensor (cf. Fig. 2b) with basal channel geometries (average over 1 m long slice) as well as flow surface and measured cross-sectional area for the intermediate scenario.
b) Investigated channel segment with approximate locations of the analyzed cross-sections (upstream of sensor distance y in meters). The red dots indicate the LiDAR point cloud projected on the camera image. Only cross-sections $y = 15$ m and $y = 5$ m will be analyzed in detail herein (Fig. 4).

2.1 Front and surface velocity

The high-resolution timelapse point clouds allowed us to identify features in the moving debris flow such as the flow front as well as large rolling boulders and woody debris. These features were labelled manually by fitting cuboids around them in every fifth point cloud frame (i.e. at a frequency of 2 Hz) using Matlab's *ground-TruthLabeler*. From the 3D Euclidean distance between subsequent cuboid positions and the corresponding timespan (i.e. 0.5 s), we calculated the 3D velocity of the front as well as of rolling boulders and woody debris.

In addition to these manual measurements, an algorithm for automated surface velocity measurement was developed. The algorithm provides the (mean) surface velocity as 3D vector field, which covers the entire investigated channel segment (Fig. 2b) at any time during the event and is based on fusing video camera and LiDAR data, as described in detail in [8].

2.2 Cross-sectional area

The cross-sectional area of the flow was determined at several locations along the channel (Fig. 2b) considering three different basal channel geometry scenarios (Fig. 2a). In the upstream sections (upstream of sensor distances $y = 25$ m and 20 m), the cross section could be measured in the LiDAR data directly by fitting a bounding area (using Matlab's *alphaShape* function) between the current debris-flow surface and the base of the flow. For the more downstream sections ($y = 15$ m, 10 m, 5 m and 0 m), point clouds acquired from photogrammetric drone flights prior and after the event were used as basal channel geometry because the LiDAR's field of view does not cover the entire channel width (Fig. 2b). For the same reason, the debris-flow surface had to be extrapolated from the middle of the channel to the banks for these four sections before fitting the bounding area. The errors introduced by the extrapolation are small because the flow surface was largely horizontal in this event (cf. also Fig. 2a).

2.3 Discharge and event volume

The discharge was estimated by multiplying the surface velocities by the cross-sectional area. For the surface velocity we used the mean value across a channel section (Fig. 2b), while for the cross-sectional area we considered the value derived from the intermediate channel geometry (Fig. 2a). We note that this approach assumes a constant bed geometry and plug-flow velocity profile, which are important assumptions and will be discussed in Section 4. If there are spatial variations in bed geometry and/or the velocity profile, we expect that the estimated discharge through these cross sections will not be the same. To quantify this, we further calculated the ratio between the discharge estimates obtained for the various cross sections.

The event volume was derived by integrating the discharge over the entire duration of the event. Because our discharge values are not continuous but discrete in time, the volume was calculated as Riemann sum over subintervals of 1 s.

3 Results

3.1 Front and surface velocity

As indicated in Figure 3, the velocity of the debris-flow front changes within the investigated channel segment. In a first phase (01:47–01:54) the front is moving at 1.2 m/s, whereas in a second phase (01:54–02:04),
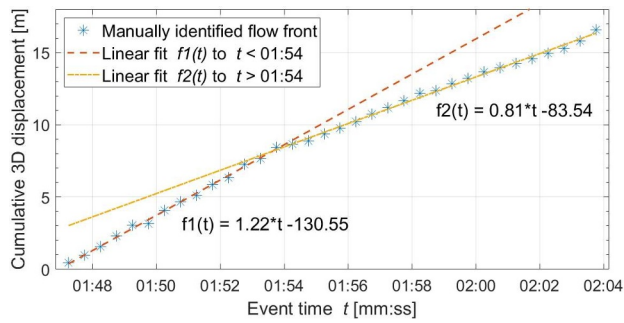
Fig. 3. Trajectory of the flow front from the 19 Sept. 2021 event, manually identified in the LiDAR point-cloud frames. The slopes of the linear trendlines indicate the change in front velocity from 1.2 m/s in a first phase (01:47–01:54) to 0.8 m/s in a second phase (01:54–02:04).

which begins roughly 5 m upstream of the sensor (cf. Fig. 2b), the front decelerates to 0.8 m/s.

We also manually measured the mean velocity of different surface features. During the first surge of the event (02:04–07:00), rolling boulders and floating woody debris were moving at similar velocities, ranging from 1.2 m/s to 1.9 m/s. However, in the second surge (07:00–13:00), the velocity of the rolling boulders was substantially slower (1.5 m/s–2.2 m/s) than the velocity of the woody debris (2.6 m/s–3.6 m/s). The ratio of these two feature velocities during the second surge was approximately 0.6 (i.e. $v_{boulder} \approx 0.6\ v_{wood}$). Manual measurements later in the event could not be performed due to a lack of identifiable surface features.

Spatially and temporally much more detailed measurements of the surface velocity were obtained in the automated analysis, which is described in detail in [8]. The automated measurements follow the general trend over time, which was already observed in the manual measurements, i.e. the surface velocities were slower (1.2 m/s–2.3 m/s) during the first surge (up to 07:00) than in the second surge of the event (1.5 m/s–3.1 m/s). Furthermore, the automated analysis also revealed a spatial variation in the surface velocity along the investigated channel segment.

3.2 Cross-Sectional area

The cross-sectional area in the more upstream sections (i.e. y = 25 m, 20 m and 15 m; cf. Fig. 2b) was between 10 m^2 (post-event channel geometry) and 13 m^2 (pre-event channel geometry) during the passage of the front. Afterwards, the cross-sectional area slightly decreased to 7 m^2–10 m^2, before increasing again after 07:00 to values between 9 m^2 and 12 m^2. Then, the cross-sectional area started decreasing relatively steadily and fell below 1 m^2 at around 25:00.

In the sections closer to the check dam (i.e. y = 5 m and 0 m), the cross-sectional area shows a similar trend over time. However, all values are generally between 3 m^2 and 5 m^2 smaller than in the more upstream sections., i.e. we observed a general decrease in cross-sectional area towards the check dam, which will be discussed below (Sect. 4).
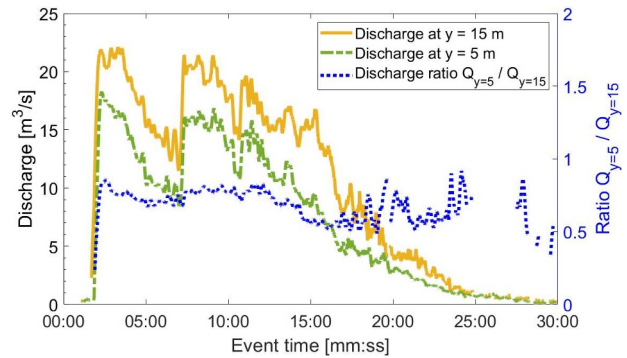

Fig. 4. Discharge estimates for the 19 Sept. 2021 debris flow at sections 15 m and 5 m upstream of the sensor (cf. Fig. 2b). The ratio $Q(y=5)/Q(y=15)$ is also indicated to highlight spatial variations in bed geometry and/or velocity profile.

3.3 Discharge

The discharge shown in Figure 4 was estimated for the sections at 15 m and 5 m upstream of the sensor, based on the automated surface velocity measurements (assuming a plug-flow velocity profile) and the intermediate channel geometry scenario (cf. Sect. 2). The discrepancy between the calculated discharge for the two different channel sections is roughly 5 m^3/s (Fig. 4) and is mainly related to the abovementioned decrease in cross-sectional area towards the check dam. The underlying assumptions and the implications of this observation will be discussed in Section 4.

Figure 4 also shows the ratio between the more downstream (y = 5 m) and the more upstream (y = 15 m) discharge estimates. Over the first 15 minutes of the event, this ratio is between 0.7 and 0.8 before slightly dropping to 0.5–0.6. As will be discussed in Section 4, this indicates that the channel bed and/or velocity profile are spatially and temporally variable.

3.4 Event volume

Based on the two discharge estimates shown in Figure 4, we calculated the volume of the 19 Sept. 2021 debris flow (cf. also Sect. 2.4). For the section at y = 15 m we calculated a volume of 17 500 m^3, whereas for the section at y = 5 m we obtained 12 500 m^3. It is important to note that this volume range is most likely a maximum estimate because we assumed a plug-flow velocity profile, i.e. a maximal depth-averaged velocity value (see also Sect. 4).

4 Discussion

The observed decrease in the front velocity (Fig. 3) by ca. 0.4 m/s could be explained by a change in the channel slope and a widening of the channel cross section. The mean channel slope in the segment 10 m to 20 m upstream of the sensor is 4.2° and the channel width is 7 m–9 m, whereas in the segment from 0 m to 10 m the slope reduces to 1.9° and the channel width increases to 12 m–14 m.

The spatial changes of surface velocity along the channel are most likely related to the presence of the check dam. The decrease in flow depth (cross-sectional area) towards the check dam is also likely caused by the check dam, which is analogous to the hydraulic drawdown upstream of a critical flow section observed in river flow (e.g. [11]).

The uncertainty of the cross-sectional area caused by the unknown shape of the channel bed during the flow is about 3 m^2 (difference in cross section assuming pre-event and post-event channel geometry). Nevertheless, the differences in the cross-sectional area between the upstream and downstream sections (e.g. $y = 25$ m and $y = 0$ m differ by 3 m^2–5 m^2 over most of the event) exceed this qualitatively-assessed uncertainty value, indicating that topographic uncertainties alone cannot explain the observed decrease in cross-sectional area towards the check dam.

Based on our calculations, the discharge in the investigated channel section decreases towards the check dam (Fig. 4), which would imply deposition of a large amount of material, not observed in the LiDAR and video data. As mentioned in Section 2.3, this discrepancy could be due to either a change in the velocity profile along the channel and/or a change in the height of the channel bed during the event. In the first case, the depth-averaged velocity of the upstream section ($y = 15$ m) would have to be reduced by a factor of 0.6–0.8 (i.e. the discharge ratio shown in Fig. 4) and would no longer be characterized by a plug-flow velocity profile. In the second case, the cross-sectional area at $y = 15$ m would be reduced by the same factor (cf. Fig. 4), which could be caused by sediment deposition during (an early phase of) the event. At present, it is difficult to separate these two effects, but they will be investigated in future events.

As mentioned in Section 3.4, our volume estimates represent maximum values because we assumed a plug-flow velocity profile for the calculation of the discharge. Therefore, the actual event volume might be smaller than our estimates. Furthermore, the volume range of ca. 5 000 m^3 provides an uncertainty assessment of our volume estimates related to the variable bed geometry and velocity profile, and it underlines the importance of investigating and better understanding these spatial variations in order to further reduce this uncertainty in the future.

5 Conclusions and outlook

In this study, hazard-related debris-flow parameters were measured with unprecedented detail at the field-scale using a novel high-resolution, high-frequency 3D timelapse LiDAR sensor. The sensor was installed at the Illgraben catchment and recorded point clouds during one debris-flow event (19 Sept. 2021), which were analyzed using both manual as well as automated methods. In our velocity measurements, we documented a decrease in the front velocity by 0.4 m/s over a ca. 25 m long channel segment and observed changes in the surface velocity during the event. Furthermore, we

tracked individual features such as large rolling boulders and woody debris and showed that the former feature was moving at roughly 0.6 the velocity of the latter during the second surge of the event (i.e. $v_{boulder} \approx 0.6\ v_{wood}$). In addition, we analyzed the discharge in various sections (assuming plug-flow and a mean channel bed geometry) upstream of a check dam and observed a decreasing discharge (3 m^3/s–5 m^3/s) towards the check dam. This "discharge paradox" could potentially be explained by an along-channel change in the velocity profile and a changing channel bed elevation during the event.

In order to better understand the fundamental mechanisms and to quantify spatial variations in velocity profiles as well as bed geometry, further investigations are necessary and will be carried out over the course of the next year based on additional field-scale LiDAR data from the Illgraben.

References

1. D.F. VanDine, Can. Geotech. J. **22**, 1 (1985)

2. O. Hungr, S. Leroueil, L. Picarelli. Landslides. **11**, 2 (2014)

3. O. Hungr. Earth Surf. Process. Landf. **25**, 5 (2000)

4. R.M. Iverson, M. Logan, R.G. LaHusen, M. Berti, J. Geophys. Res. Earth Surf. **115**, F3 (2010)

5. M. Hürlimann, V. Coviello, C. Bel, X. Guo, M. Berti, C. Graf, J. Hübl, S. Miyata, J.B. Smith, H.-Y. Yin, Earth-Sci. Rev. **199** (2019)

6. R. Kaitna, W.E. Dietrich, L. Hsu, J. Fluid Mech. **741** (2014)

7. G. Nagl, J. Hübl, R. Kaitna, Earth Surf. Process. Landf. **45** (2020)

8. J. Aaron, R. Spielmann, B.W. McArdell, *Debris flow monitoring with high-frequency 3D LiDAR scanners: a new method to infer the internal dynamics of debris flows*, 8th International Conference on Debris Flow Hazard Mitigation, DFHM8, 26-29 June 2023, Torino, Italy (submitted)

9. B.W. McArdell, M. Sartori, *The Illgraben Torrent System*, in Landscapes and Landforms of Switzerland (Springer International Publishing, Cham, 2021)

10. M. Jacquemart, L. Meier, C. Graf, F. Morsdorf, Nat. Hazards, **89**, 2 (2017)

11. F.M. Henderson, *Open Channel Flow* (Macmillan, New York, 1966)